Fundaments of optical far-field subwavelength resolution based on illumination with surface waves

Roberto Lopez-Boada,[1] Charles J. Regan,[2,3] Daniel Dominguez,[3,4] Ayrton. A. Bernussi,[2,3] and Luis Grave de Peralta[3,4,*]

[1]*ACE, Barry University, Miami Shores, FL 33161, USA*
[2]*Department of Electrical and Computer Engineering, Texas Tech University, Lubbock, TX 79409, USA*
[3]*Nano Tech Center, Texas Tech University, Lubbock, TX 79409, USA*
[4]*Department of Physics, Texas Tech University, Lubbock, TX 79409, USA*
[*]*luis.grave-de-peralta@ttu.edu*

Abstract: We present a general discussion about the fundamental physical principles involved in a novel class of optical superlenses that permit to realize in the far-field direct non-scanning images with subwavelength resolution. Described superlenses are based in the illumination of the object under observation with surface waves excited by fluorescence, the enhanced transmission of fluorescence via coupling with surface waves, and the occurrence of far-field coherence-related fluorescence diffraction phenomena. A Fourier optics description of the image formation based on illumination with surface waves is presented, and several recent experimental realizations of this technique are discussed. Our theoretical approach explains why images with subwavelength resolution can be formed directly in the microscope camera, without involving scanning or numerical post-processing. While resolution of the order of λ/7 has been demonstrated using the described approach, we anticipate that deeper optical subwavelength resolution should be expected.

OCIS codes: (110.0180) Microscopy; (240.6680) Surface plasmons; (240.6690) Surface waves; (260.2510) Fluorescence; (260.6970) Total internal reflection.

References and links

1. S. Durant, Z. Liu, J. M. Steele, and X. Zhang, "Theory of the transmission properties of an optical far-field superlens for imaging beyond the diffraction limit," J. Opt. Soc. Am. B **23**(11), 2383–2392 (2006).
2. E. Hetcht, *Optics*, 3rd edition (Addison Wesley, 1998).
3. M. Born and E. Wolf, *Priciples* of *Optics*, 5th edition (Pergamon Press, 1975).
4. J. B. Pendry, "Negative refraction makes a perfect lens," Phys. Rev. Lett. **85**(18), 3966–3969 (2000).
5. D. O. S. Melville, R. J. Blaikie, and C. R. Wolf, "Submicron imaging with a planar silver lens," Appl. Phys. Lett. **84**(22), 4403–4405 (2004).
6. W. Srituravanich, N. Fang, C. Sun, Q. Luo, and X. Zhang, "Plasmonic Nanolithography," Nano Lett. **4**(6), 1085–1088 (2004).
7. O. E. Gawhary, N. J. Schilder, A. C. Assafrao, S. F. Pereira, and H. P. Urbach, "Restoration of s-polarized evanescen waves and subwavelength imaging by a single dielectric slab," New J. Phys. **14**(5), 053025 (2012).
8. Y. Zhang, C. Arnold, P. Offermans, and J. Rivas, "Surface wave sensors based on nanometric layers of strongly absorbing materials," Opt. Express **20**(9), 9431–9441 (2012).
9. Z. Liu, S. Durant, H. Lee, Y. Pikus, N. Fang, Y. Xiong, C. Sun, and X. Zhang, "Far-field optical superlens," Nano Lett. **7**(2), 403–408 (2007).
10. Z. Liu, H. Lee, Y. Xiong, C. Sun, and X. Zhang, "Far-field optical hyperlens magnifying sub-diffraction-limited objects," Science **315**(5819), 1686 (2007).
11. X. Zhang and Z. Liu, "Superlenses to overcome the diffraction limit," Nat. Mater. **7**(6), 435–441 (2008).
12. R. Rodriguez, C. J. Regan, A. Ruiz-Columbié, W. Agutu, A. A. Bernussi, and L. Grave de Peralta, "Study of plasmonic crystals using Fourier-plane images obtained with plasmon tomography far-field superlenses," J. Appl. Phys. **110**(8), 083109 (2011).

13. C. J. Regan, R. Rodriguez, S. C. Gourshetty, L. Grave de Peralta, and A. A. Bernussi, "Imaging nanoscale features with plasmon-coupled leakage radiation far-field superlenses," Opt. Express **20**(19), 20827–20834 (2012).
14. N. Garcia and M. Nieto-Vesperinas, "Left-handed materials do not make a perfect lens," Phys. Rev. Lett. **88**(20), 207403 (2002).
15. C. J. Regan, D. Dominguez, A. A. Bernussi, and L. Grave de Peralta, "Far-field optical superlens without metal," J. Appl. Phys. ((to be published).
16. M. H. Raether, *Surface Plasmons on Smooth and Rough Surfaces and on Gratings* (Springer-Verlag, 1988).
17. G. Christou and C. Mias, "Critique of optical negative refraction superlensing," Plasmonics **6**(2), 307–309 (2011).
18. S. P. Frisbie, C. Chesnutt, M. E. Holtz, A. Krishnan, L. de Peralta, and A. A. Bernussi, "Image formation in wide-field microscopes based on leakage of surface plasmon-coupled fluorescence," IEEE Photon. J. **1**(2), 153–162 (2009).
19. L. Grave de Peralta, C. J. Regan, and A. A. Bernussi, "SPP tomography: a simple wide-field nanoscope," Scanning n/a (2012), doi:10.1002/sca.21057.
20. I. Gryczinski, J. Malicka, K. Nowaczyk, Z. Gryczynski, and J. Lacowicz, "Effects of sample thickness on the optical properties of surface plasmon-coupled emission," J. Phys. Chem. B **108**(32), 12073–12083 (2004).
21. I. Gryczynski, J. Malicka, Z. Gryczynski, and J. R. Lakowicz, "Surface plasmon-coupled emission with gold films," J. Phys. Chem. B **108**(33), 12568–12574 (2004).
22. F. Goos and H. Hänchen, "Ein neuer und fundamentaler versuch zur totalreflexion," Ann. Phys. **6**(7-8), 333–346 (1947).
23. S. A. Taya, E. J. El-Farram, and T. M. El-Agez, "Goos-Hänchen shift as a probe in evanescent slab waveguides sensors," Int. J. Electron. Commun. **66**(3), 204–210 (2012).
24. J. W. Goodman, *Introduction to Fourier Optics* (McGraw-Hill, 1968).
25. A. Drezet, A. Hohenau, D. Koller, A. Stepanov, H. Ditlbacher, B. Steinberger, F. R. Aussenegg, A. Leitner, and J. R. Krenn, "Leakage radiation microscopy of surface plasmon polaritons," Mater. Sci. Eng. B **149**(3), 220–229 (2008).
26. L. Grave de Peralta, R. Lopez-Boada, A. Ruiz-Columbie, S. Park, and A. A. Bernussi, "Some consequences of experiments with a plasmonic quantum eraser for plasmon tomography," J. Appl. Phys. **109**(2), 023101 (2011).
27. A. Houk, R. Lopez-Boada, A. Ruiz-Columbie, S. Park, A. A. Bernussi, and L. Grave de Peralta, "Erratum: some consequences of experiments with a plasmonic quantum eraser for plasmon tomography," J. Appl. Phys. **109**(11), 119901 (2011).
28. J. J. Burke, G. I. Stegeman, and T. Tamir, "Surface-polariton-like waves guided by thin, lossy metal films," Phys. Rev. B Condens. Matter **33**(8), 5186–5201 (1986).
29. Z. Liu, N. Fang, T. Yen, and X. Zhang, "Rapid growth of evanescent wave by silver superlens," Appl. Phys. Lett. **83**(25), 5184–5186 (2003).
30. F. L. Pedrotti, L. S. Pedrotti, and L. M. Pedrotti, *Introduction to Optics*, 3rd Edition (Person Prentice Hall, 2007).
31. B. Schumacher, *Quantum mechanics: the Physics of the Microscopic World* (The Teaching Company, 2009).
32. E. J. Galvez, C. H. Holbrow, M. J. Pysher, J. W. Martin, N. Courtemanche, L. Heilig, and J. Spencer, "Interference with correlated photons: five quantum mechanics experiments for undergraduates," Am. J. Phys. **73**(2), 127–140 (2005).
33. L. Grave de Peralta, "Phenomenological quantum description of the ultra fast response of arrayed waveguide gratings," J. Appl. Phys. **108**(10), 103110 (2010).
34. Y. Chen, D. Zhang, L. Han, G. Rui, X. Wang, P. Wang, and H. Ming, "Surface-plasmon-coupled emission microscopy with a polarization converter," Opt. Lett. **38**(5), 736–738 (2013).
35. W. T. Tang, E. Chung, Y. H. Kim, P. T. C. So, and C. J. Sheppard, "Surface-plasmon-coupled emission microscopy with a spiral phase plate," Opt. Lett. **35**(4), 517–519 (2010).
36. C. J. Regan, O. Thiabgoh, L. Grave de Peralta, and A. A. Bernussi, "Probing photonic Bloch wavefunctions with plasmon-coupled leakage radiation," Opt. Express **20**(8), 8658–8666 (2012).
37. C. J. Regan, L. Grave de Peralta, and A. A. Bernussi, "Equifrequency curve dispersion in dielectric-loaded plasmonic crystals," J. Appl. Phys. **111**(7), 073105 (2012).
38. C. J. Regan, A. Krishnan, R. Lopez-Boada, L. Grave de Peralta, and A. A. Bernussi, "Direct observation of photonic Fermi surfaces by plasmon tomography," Appl. Phys. Lett. **98**(15), 151113 (2011).
39. J. D. Joannopoulus, S. G. Johnson, J. N. Winn, and R. D. Meade, *Photonic Crystals: Molding the Flow of Light* (Princeton University, 2008).

1. Introduction

The conventional wisdom, formed from the Abbe's theory of image formation and Fourier optics, is that traditional optical microscopy is diffraction-limited to spatial periods (p) larger than ~λ_o/NA [1,2], or separation between two points (Δx) larger than $\lambda_o/(2NA)$ [1–3], where NA is the numerical aperture of the microscope objective lens, and λ_o is the free space wavelength of the illuminating light. This explain why the theoretical prediction that a simple thin layer of metal could be used to realize a practical superlens [4] was warmly received by the optical community searching for novel imaging techniques with subwavelength resolution for nanotechnology and subcellular biological applications. Since then, optical subwavelength resolution in the near-field using metallic superlenses has been demonstrated [5,6], exciting new near-field superlenses without metal have been also proposed [7,8], and the original concept was extended to the far-field [9–13]. Some demonstrated far-field superlenses require intensive numerical image post processing [1,9], some require a structure much more complicated than the original Pendry's proposal [10], but until recently, all demonstrated far-field superlenses require a structure with at least a thin metal layer. The unavoidable inherent losses associated with the presence of the metal layer constitute a drawback characteristic of these superlenses [14]; therefore, alternative methods for mitigation of the metal-related losses are of great interest.

Recently, the first far-field optical superlens without metal has been demonstrated. The details of the experiments will be published elsewhere [15]. While investigating the physical principles responsible for the subwavelength resolution capabilities of the far-field superlenses that resemble more closely the original Pendry's proposal [12,13], we realized that the specific nature of the surface plasmon polaritons (SPP) [16] excited in the superlens was not a requirement for obtaining subwavelength resolution. This idea had been discussed previously in the context of near-field superlenses [7,17] but its application to realize far-field superlenses remains unexplored. In this work we show that the same physical principles are responsible for the optical subwavelength resolution capabilities of demonstrated far-field superlens without metal [15] and plasmonic superlenses [12,13]. In what follows, we group both types of far-field superlenses in the concept of "surface wave illumination" superlenses (SWIS). We show that the optical far-field subwavelength resolution obtained using SWIS is based on three common principles: the illumination of the object under observation with surface waves excited by fluorescence, the enhanced transmission of fluorescence via coupling with surface waves, and the occurrence of far-field coherence-related fluorescence diffraction phenomena. Therefore, SWIS are not ideal superlenses in the original sense of being capable of infinite resolution [4,14,17], but they are far-field superlenses because SWIS allow direct imaging in the far-field with subwavelength resolution, without involving scanning or numerical post-processing. We present here, for the first time, a comprehensive Fourier Optics description of the image formation in a SWIS-microscope arrangement. The theory of image formation using SWIS proposed in this wok represents a generalization to far-field superlenses of the well-known Abbe's theory of image formation. This makes the design of far-field superlenses easier and more intuitive by expanding the range of applicability of the conventional wisdom about the image formation in optical instruments. For instance, we show using these ideas how it might be possible to obtain deep optical subwavelength resolution with SWIS.

This paper is organized as follows: In Section 2 we make a general description of a SWIS and discuss the phenomena of enhanced transmission of fluorescence via excitement of surface waves. Section 3 is dedicated to the Fourier optics description of the formation of the Fourier plane (FP) images obtained in a SWIS-microscope arrangement. Several simple examples are presented, and the analytical expressions are derived and compared with experimental FP images. In Section 4, a Fourier optics description of the formation of the surface emission (SE) images is presented, and the origin of the SWIS subwavelength resolution is elucidated. Finally, the conclusions of this work are given in Section 5.

2. Enhanced transmission of fluorescence coupled to surface waves

Figure 1(a) shows a schematic illustration of the rather simple transversal structure of a typical SWIS. The SWIS substrate is formed by a ~150 μm thick glass cover slip. At the top of the SWIS is a ~150 nm thick layer of PolyMethylMethAcrylate (PMMA) doped with Rhodamine-6G (R6G) with peak emission at λ_o~568 nm wavelength. As shown in Fig. 1(a), an optional ~50 nm thick gold layer may be present between the substrate and the top layer.

#186361 - $15.00 USD Received 5 Mar 2013; revised 28 Apr 2013; accepted 3 May 2013; published 8 May 2013

The object under observation (not shown in Fig. 1(a)) should be embedded in the PMMA + R6G layer. The SWIS with the object under observation is then placed in a traditional inverse microscope with an immersion oil high *NA* objective lens. A detailed description of a typical SWIS-microscope arrangement have being previously published [12,13,15,18,19].

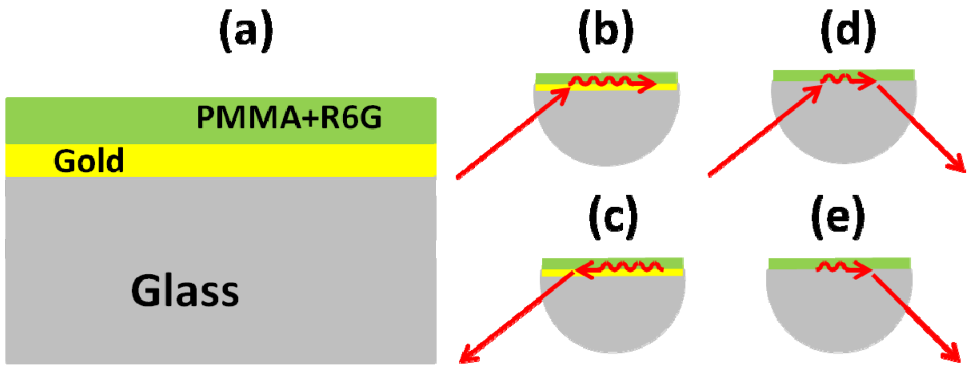

Fig. 1. (a) Cross-section schematic illustration of a sample used in a typical SWIS. (b)-(e) illustrates different excitation schemes: conventional surface wave excitation [(b) and (d)] and the excitation of the surface waves in SWIS [(c) and (e)] for superlenses with [(b) and (c)] and without [(d) and (e)] a thin metal layer.

Typically, the R6G fluorophores in the PMMA layer are excited with light of a continuous wave 532nm wavelength emitted by a diode pumped solid state laser. In SWIS, surface waves are excited in the medium/PMMA interface by spontaneous emission events occurring randomly in every direction near the interface, where the medium is gold in plasmonic superlenses [12,13] or glass in superlenses without metal [15]. The surface waves are SPP in plasmonic superlenses, or surface waves related with total internal reflection (TIR) phenomena in superlenses without metal [15]. As shown in Figs. 1(b)-1(e), in SWIS the excitation of surface waves by fluorescence results in a type of reverse phenomena when compared to more standard methods to excite the surface waves. Figure 1(b) shows a schematic illustration of SPP excitation using the well-known Kretschmann configuration [16]. As it is illustrated in Fig. 1(c), plasmonic SWIS are based on the optical reversibility principle [2], i.e., the excitation of SPP by fluorescence results in the occurrence of plasmon-coupled leakage radiation [18,20,21]. Figure 1(d) shows a schematic illustration of TIR in a conventional prism. The incident light produces a surface wave at the glass surface that travels a few microns before leaking to the glass producing the reflected light [15, 22,23]. As it is illustrated in Fig. 1(e), in SWIS without metal the output light is produced by the fluorescence-excited surface waves without the presence of an incident beam. In SWIS, the surface waves excited by fluorescence illuminate the object under observation; i.e. the surface waves are the illumination source. This is of particular importance. A well known result of the Abbe's theory of image formation and Fourier optics is that the minimum resolvable period using a traditional microscope is given by the following expression [1,2, 24]:

$$p_{\min} = \frac{\lambda_o}{NA}. \tag{1}$$

Equation (1) corresponds to a minimum resolvable separation between two points of $\Delta x \sim 0.61 p_{min}$ [1,19]. However, it is less known that Eq. (1) is derived assuming that the sample is illuminated by a coherent monochromatic plane wave that propagates perpendicularly to the surface of the sample under observation. The electric field associated with the surface waves has a more prominent component, $E_{\dagger}$, which is perpendicular to the propagation direction and can be perpendicular or parallel to the medium/PMMA interface; therefore, in

#186361 - $15.00 USD Received 5 Mar 2013; revised 28 Apr 2013; accepted 3 May 2013; published 8 May 2013
(C) 2013 OSA 20 May 2013 | Vol. 21, No. 10 | DOI:10.1364/OE.21.011928 | OPTICS EXPRESS 11931

SWIS the illumination source can be considered, in a first approximation, a superposition of plane waves propagating in all directions along the medium/PMMA interface. As a consequence, one should expect that Eq. (1) could not apply to SWIS. The component $E_{\dagger}$ of the electric field associated with a plane wave propagating along the medium/PMMA interface in the direction defined by the wavevector, $\overrightarrow{k_w}$ is described by the following expression:

$$E_{\dagger}\left(\vec{r},t\right)=E_{\dagger o}\sin\left(\overrightarrow{k_w}\cdot\vec{r}-\omega t\right), \tag{2}$$

where,

$$\left|\overrightarrow{k_w}\right|=k_w={}^{2\pi}\!/\!_{\lambda}=k_o n_{eff}\ ,\ \lambda={}^{\lambda_o}\!/\!_{n_{eff}}\ ,\ \omega=2\pi\nu. \tag{3}$$

$E_{\dagger o}$, λ, and ν are the amplitude, wavelength, and frequency of the plane wave, respectively; n_{eff} is the effective refractive index experienced by the surface wave, and $\vec{r}=(x,y)$ is contained in the plane z = 0 (medium /PMMA interface). The surface waves are continuously leaking to the glass substrate of the sample while propagating through the medium/PMMA interface [25–27]. This is the light used for imaging in a SWIS-microscope arrangement [12,13,15,18,19].

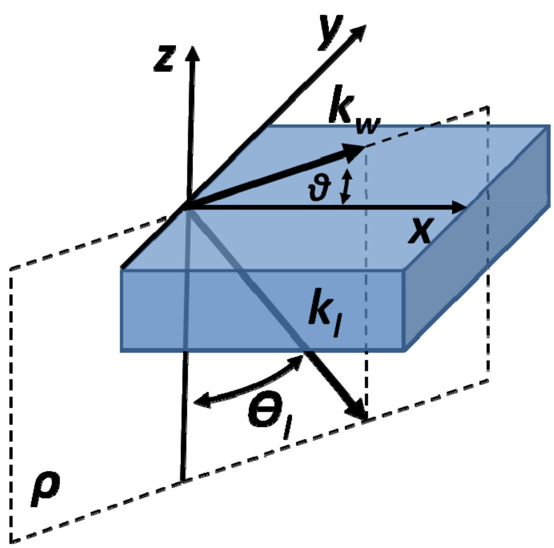

Fig. 2. Light leaks in the direction defined by $\overrightarrow{k_l}$, which forms an angle θ_l with respect to the axis z. Leaked light is contained in the plane ρ, which also contains the z axis and the vectors $\overrightarrow{k_w}$ and $\overrightarrow{k_l}$.

As shown in Fig. 2, for a given value of $\overrightarrow{k_w}$, leakage radiation is very directional. It occurs in a very narrow angle interval centered at a direction forming an angle θ_l respect to the normal to the medium/PMMA interface [20,21, 25]. Therefore, the light leaking in the direction θ_l can be described to a good approximation as a plane wave [25], which electric field (E_l) is given by the following expression:

$$E_l\left(\vec{s},t\right)=E_{lo}\sin\left(\overrightarrow{k_l}\cdot\vec{s}-\omega t\right), \tag{4}$$

#186361 - $15.00 USD Received 5 Mar 2013; revised 28 Apr 2013; accepted 3 May 2013; published 8 May 2013

where

$$\left|\overrightarrow{k_l}\right| = \sqrt{k_\perp^2 + k_\parallel^2} = 2\pi/\lambda_s\ ,\ \lambda_s = \lambda_o/n_s\ . \tag{5}$$

Here n_s is the refractive index of the substrate, $\vec{s} = (x, y, z)$, and E_{lo} is proportional to $E_{\dagger o}$ [25–28]. $k_\perp$ and $k_\parallel$ are the components of the wavevector of the leakage radiation ($\overrightarrow{k_l}$) in the direction perpendicular and parallel to the medium/PMMA interface, respectively. $\overrightarrow{k_\parallel}$ is also parallel to $\overrightarrow{k_w}$ [26], and its magnitude is given by the following expression [16,18,25]:

$$k_\parallel = k_l \sin\theta_l = k_w. \tag{6}$$

SPP surface waves have a small component of the electric field in the direction of propagation [25], which makes Eq. (2) only a first approximation of a SPP plane wave. However, Eq. (4) is still valid for a SPP wave because E_{lo} is proportional to the amplitudes of both electric field components [25]. A signature of the occurrence of enhanced transmission of fluorescence coupled to surface waves [15,20,21,29] is that the $E_{lo} / E_{\dagger o} >> E_t / E_{\dagger o}$, where E_t is the magnitude of the electric field corresponding to the fluorescence radiation that pass through the medium/PMMA interface without exciting surface waves. The surface and the leakage radiation plane waves described by the Eqs. (2) and (4), respectively, are coherent waves. This description is then appropriate only if the coherence length of the fluorescence (l_c) is larger than the propagation length of the surface waves (L). The value of l_c can be estimated using the following expression [30]:

$$l_c = \frac{\lambda_o^2}{\Delta\lambda}, \tag{7}$$

where Δλ is the spectral width of the passband filter placed after the immersion oil objective lens for filtering the laser excitation light [12,13,15,18,19]. For Δλ = 10 nm, we calculate a value of l_c ~30 µm, which is larger than the values of L~20µm [16,25,26] and few µm [22,23] for SPP and surface waves related to TIR, respectively. Therefore, it is well justified to consider that in SWIS the sample is illuminated in the direction determined by $\overrightarrow{k_w}$ by a coherent surface wave excited by fluorescence.

3. Formation of the Fourier plane images

3.1 Homogeneous sample

For a SWIS without object under observation, the optical disturbance (U) at the medium/PMMA interface (z = 0) associated to E_l is given by the following expression [24]:

$$U_\varphi(x, y, z=0) = C_\varphi e^{i\overrightarrow{k_w}\cdot\vec{r}} = C_\varphi e^{i(xk_w\cos\varphi + yk_w\sin\varphi)}, \tag{8}$$

where C_φ is a real constant, i is the imaginary unit, and φ is the angle between $\overrightarrow{k_w}$ and the x-axis (see Fig. 2). $\overrightarrow{k_w} = 0$ corresponds to a plane wave traversing perpendicularly and undisturbed through the plane z = 0; therefore, the phase factor $e^{i\overrightarrow{k_w}\cdot\vec{r}}$ carries the information about the directionality of the leakage radiation associated to a plane wave propagating in the direction defined by $\overrightarrow{k_w}$ along the medium/PMMA interface. The optical disturbance at the Fourier plane (FP), $U_\varphi(k_x,k_y)$, is given by the Fourier Transform (*FT*) of $U_\varphi(x,y,z = 0)$ [24], i.e.:

$$U_\varphi(k_x,k_y) \propto FT\left[U_\varphi(x,y,z=0)\right] \propto \iint U_\varphi(x,y,z=0)e^{-i\left(xk_x+yk_y\right)}dxdy. \tag{9}$$

Here $k = 2\pi/\Lambda$ and $1/\Lambda$ is the spatial frequency. Using Eqs. (8) and (9) results, for the excitation in a homogeneous sample of the surface wave described by Eq. (2), the following expression:

$$\begin{aligned} U_\varphi(k_x,k_y) &\propto \iint C_\varphi e^{-i\left[\left(k_x-k_w\cos\varphi\right)x+\left(k_y-k_w\sin\varphi\right)y\right]}dxdy \\ &\propto \delta(k_x-k_w\cos\varphi,\ k_y-k_w\sin\varphi). \end{aligned} \tag{10}$$

Where δ(k) is the delta of Dirac function [24]. The intensity distribution at the FP is proportional to the square of the absolute value of $U_\varphi(k_x,k_y)$, i.e.:

$$I_\varphi(k_x,k_y) \propto \left|U_\varphi(k_x,k_y)\right|^2. \tag{11}$$

From Eqs. (9)-(11) then follows that:

$$I_\varphi(k_x,k_y) \propto \delta^2(k_x-k_w\cos\varphi,\ k_y-k_w\sin\varphi). \tag{12}$$

The intensity distribution in the FP images obtained in the SWIS-microscope arrangement [12,13,15,18,19] is the part of $I_\varphi(k_x,k_y)$ inside of the reciprocal space region captured by the microscope objective lens, $\left|\vec{k}\right| \le k_o NA$; i.e.:

$$I_{\varphi,FPI}(k_x,k_y) \begin{array}{ll} =0, & \left|\overrightarrow{k_w}\right| > k_o NA \\ \propto \delta^2(k_x-k_w\cos\varphi,\ k_y-k_w\sin\varphi), & \left|\overrightarrow{k_w}\right| \le k_o NA \end{array}, \tag{13}$$

Therefore, the intensity distribution in a FP image, corresponding to the excitation in a homogeneous sample of the surface wave described by Eq. (2), is a bright spot at the reciprocal space point $\left(k_w\cos\varphi, k_w\sin\varphi\right)$ at the extreme of the vector $\vec{k} = \overrightarrow{k_w}$. Basically, $I_{\varphi,FPI}(k_x,k_y)$ is the observed far-field diffraction pattern, which is produced by the interference between photons that leaks from the medium/PMMA interface in the direction defined by $\overrightarrow{k_w}$. The interference occurs because it is impossible to know the path of the photons arriving to the FP image at the spot $\left(k_w\cos\varphi, k_w\sin\varphi\right)$. I.e., photons that leaks in the direction, φ, through different points in the medium/PMMA interface, and arrive to the same spot in the FP image, are undistinguishable; therefore, they interfere [31–33]. However, photons that leaks in different directions can be distinguished by the direction of their momenta; thus, they cannot interfere [31–33]. In consequence, the total intensity at the FP, $I_T(k_x,k_y)$, must be calculated by adding the intensity contributions $I_\varphi(k_x,k_y)$ corresponding to all the surface waves illumination directions φ; i.e, $I_T(k_x,k_y)$ is described by the following expression:

$$I_T(k_x,k_y) = \sum_\varphi I_\varphi(k_x,k_y). \tag{14}$$

#186361 - $15.00 USD Received 5 Mar 2013; revised 28 Apr 2013; accepted 3 May 2013; published 8 May 2013

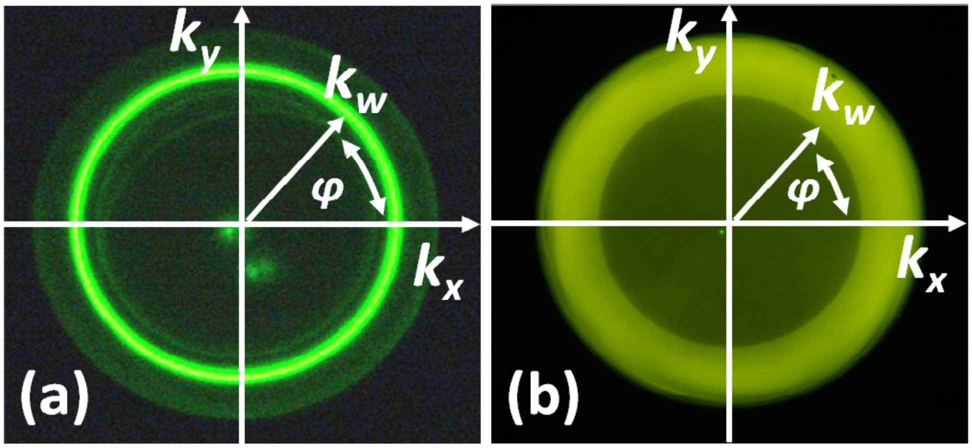

Fig. 3. FP images obtained with a SWIS-microscope arrangement corresponding to a uniform sample where (a) SPPs and (b) surface waves related to TIR, were excited. When the direction of propagation of the surface waves along the medium/PMMA interface, φ, changes from 0 to 2π, $\vec{k}_w$ rotates describing a ring.

Consequently, assuming that $|\vec{k}_w| \le k_o NA$, for a homogeneous sample the intensity distribution in the FP image is a bright ring of radius $k = k_w$ centered at the origin of the reciprocal space. Figure 3 shows FP images obtained with a SWIS-microscope arrangement corresponding to two homogeneous samples [15,18]. A thin (thick) bright ring in Fig. 3(a) (3(b)) corresponds to the enhanced transmission of fluorescence coupled to SPP [20,21,29] (surface waves related to TIR [15]). The weak background in the FP images is produced by the fluorescence that passed through the medium/PMMA interface without exciting surface waves. The difference in brightness between the rings and the background corresponds to the fluorescence enhancement transmission condition $E_{lo} / E_{\dagger o} >> E_t / E_{\dagger o}$. As illustrated in Fig. 3, when the direction φ of the surface wave illumination changes from 0 to 2π, the vector $\vec{k}_w$ rotates describing a ring. The width of the thin ring in Fig. 3(a) is not zero because in reality the propagation length of a lossy surface wave is not infinite, as it is implicit in Eq. (2), but finite. As a consequence, the leakage radiation occurs in a very narrow but finite angle interval [20,21,25], the spot $(k_w \cos\varphi, k_w \sin\varphi)$ gets elongated in the radial direction, and the transversal section of the ring exhibits a Lorentzian profile with a width inverse proportional to the propagation length of the surface wave [25]. The thick ring in Fig. 3(b) corresponds to the occurrence of TIR for a broad range of incident angles [15]. This is because, as sketched in Figs. 1(e) and 1(d), surface waves are excited by the fluorescence with a different value of k_w for every angle larger than the TIR angle. It should be pointed out that the sum of intensities in Eq. (14) is different than alternative approaches where the electric field amplitudes corresponding to light leaked in different directions were added [34,35]. A comprehensive study of this apparent discrepancy will be published elsewhere.

3.2 Periodic sample

For a sample with a sinusoidal profile of period p along the x axes, the optical disturbance (U) at the gold/PMMA interface (z = 0) associated to E_l is proportional to the Bloch wavefunction corresponding to the periodical structure, i.e [36]:

#186361 - $15.00 USD Received 5 Mar 2013; revised 28 Apr 2013; accepted 3 May 2013; published 8 May 2013

$$U_{\varphi,p}(x,y,z=0)=C_{\varphi}\left[1+\sin\left(\tfrac{2\pi}{p}x\right)\right]e^{i\overrightarrow{k_w}\cdot\vec{r}}$$
$$=C_{\varphi}\left[1+\sin\left(\tfrac{2\pi}{p}x\right)\right]e^{i\left(xk_w\cos\varphi+yk_w\sin\varphi\right)}. \tag{15}$$

From Eqs. (9) and (15) follows that the optical disturbance at the FP is now given by the following expression:

$$U_{\varphi,p}(k_x,k_y)\propto\iint C_{\varphi}\left[1+\sin\left(\tfrac{2\pi}{p}x\right)\right]e^{-i\left[\left(k_x-k_w\cos\varphi\right)x+\left(k_y-k_w\sin\varphi\right)y\right]}dxdy. \tag{16}$$

Thus:

$$U_{\varphi,p}(\vec{k})\propto\left\{\delta\left[\vec{k}-\overrightarrow{k_w}\right]+\delta\left[\vec{k}-\left(\vec{G}+\overrightarrow{k_w}\right)\right]+\delta\left[\vec{k}-\left(-\vec{G}+\overrightarrow{k_w}\right)\right]\right\}, \tag{17}$$

where $\vec{G}$ is the reciprocal lattice vector corresponding to the grating, i.e.:

$$\left|\vec{G}\right|=G=\tfrac{2\pi}{p}. \tag{18}$$

$U_{\varphi,p}(\vec{k})$ is a shifted version of the optical disturbance corresponding to the far-field two-dimensional diffraction pattern that would be obtained under traditional out-of-plane perpendicular illumination [24]. Therefore, Eq. (16) can be rewritten as:

$$U_{\varphi,p}(\vec{k})=U_{\perp,p}(\vec{k}-\overrightarrow{k_w}), \tag{19}$$

where:

$$U_{\perp,p}(\vec{k})\propto\left\{\delta\left[\vec{k}\right]+\delta\left[\vec{k}-\vec{G}\right]+\delta\left[\vec{k}+\vec{G}\right]\right\}. \tag{20}$$

Consequently, if $k_w+G\le k_oNA$, the BFP image is formed by three bright spots at the reciprocal space points $\left(k_w\cos\varphi,k_w\sin\varphi\right)$, $\left(k_w\cos\varphi+G,k_w\sin\varphi\right)$, and $\left(k_w\cos\varphi-G,k_w\sin\varphi\right)$ at the extreme of the vectors $\overrightarrow{k_w}$, $\vec{G}+\overrightarrow{k_w}$, and $-\vec{G}+\overrightarrow{k_w}$, respectively. Substituting Eq. (19) into Eq. (14) permits to calculate the total intensity distribution at the FP, $I_T(k_x,k_y)$, corresponding to the incoherent superposition of numerous plane waves propagating in all directions along the medium/PMMA interface.

Figure 4 shows a FP image corresponding to a plasmonic sample with a periodic profile along the *x*-axis, with p = 4 μm, for a case where $k_w+G<k_oNA$ [18]. As shown in Fig. 4, when the direction φ of the surface waves illumination changes from 0 to 2π, the vectors $\overrightarrow{k_w}$ with origin at the points $(0,0)$, $(+G,0)$, and $(-G,0)$ rotate simultaneously around their origins. As a consequence, the three spots $\left(k_w\cos\varphi,k_w\sin\varphi\right)$, $\left(k_w\cos\varphi+G,k_w\sin\varphi\right)$, and $\left(k_w\cos\varphi-G,k_w\sin\varphi\right)$ simultaneously describe circumferences of radius k_w centered at the points $(0,0)$, $(+G,0)$, and $(-G,0)$, respectively. Due to the non-sinusoidal profile of the sample, in addition to the zero and first order rings, two arc-segments of the second order rings centered at the points $(+2G,0)$, and $(-2G,0)$ can be seen in the FP image shown in Fig. 4. The second order rings do not appear complete because in the FP image only appears the fraction of the total intensity distribution $I_T(k_x,k_y)$, which is inside of the reciprocal space region $\left|\vec{k}\right|\le k_oNA$.

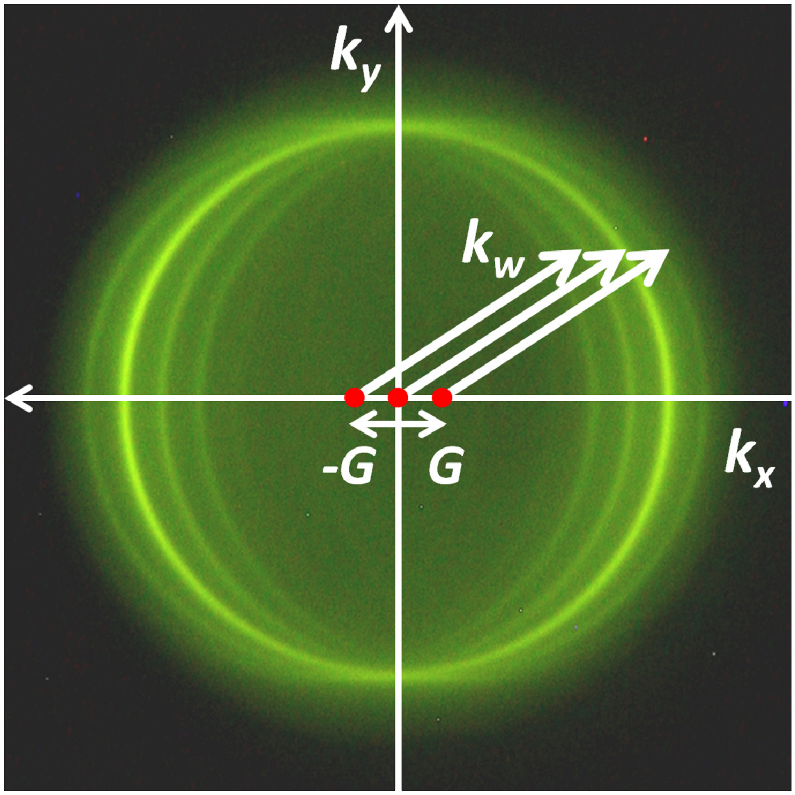

Fig. 4. FP image corresponding to a plasmonic sample with a periodic profile along the *x*-axis, with p = 4 μm. When the direction φ of the surface waves illumination changes from 0 to 2π, the extreme of each vector $\overrightarrow{k_w}$ describes a circumference.

3.3 General case

In general, the optical disturbance at the medium/PMMA interface corresponding to a single plane wave propagating along the medium/PMMA interface is given by the following expression:

$$U_\varphi(x,y,z=0)=f(x,y)e^{i\overrightarrow{k_w}\cdot\vec{r}}=f(x,y)e^{i(xk_w\cos\varphi+yk_w\sin\varphi)},\tag{21}$$

where *f(x,y)* is the optical disturbance at the medium/PMMA interface that would exist under traditional perpendicular out-of-plane illumination. The corresponding optical disturbance at the FP is then given by the following expression:

$$U_\varphi(k_x,k_y)\propto\iint f(x,y)e^{-i\left[(k_x-k_w\cos\varphi)x+(k_y-k_w\sin\varphi)y\right]}dxdy.\tag{22}$$

Therefore, $U_\varphi(\vec{k})$ is proportional to the two-dimensional FT of *f(x,y)* after a translation in the reciprocal space by $\overrightarrow{k_w}$, i.e.:

$$U_\varphi(\vec{k})=U_\perp(\vec{k}-\overrightarrow{k_w}),\tag{23}$$

where, $U_\perp(\vec{k})$ would be the optical disturbance at the medium/PMMA interface if the sample was traditionally studied with perpendicular out-of-plane illumination i.e.:

#186361 - $15.00 USD Received 5 Mar 2013; revised 28 Apr 2013; accepted 3 May 2013; published 8 May 2013

$$U_{\perp}(\vec{k}) \propto FT\left[f(x,y)\right] \propto \iint f(x,y)e^{-i\vec{k}\cdot\vec{r}}dxdy. \tag{24}$$

In general, $U_{\varphi}(\vec{k})$ is different than zero in a large area, therefore $U_{\varphi}(\vec{k})$ is not an slide in the direction φ of the BFP image as it was proposed in Ref. 18. The intensity distribution $I_{\varphi}(\vec{k})$ at the FP corresponding to $U_{\varphi}(\vec{k})$ is given by the Eq. (11). The total intensity distribution at the FP, $I_T(\vec{k})$, must be obtained by adding the intensity contributions $I_{\varphi}(\vec{k})$ corresponding to all the surface waves illumination directions φ; therefore, it is described by the Eq. (14). Consequently, from Eqs. (11) and (14), and Eq. (24) we obtain:

$$I_T(\vec{k}) \approx \sum_{\varphi} a_{\varphi}\left|U_{\perp}(k_x - k_w\cos\varphi, k_y - k_w\sin\varphi)\right|^2. \tag{25}$$

Each term $a_{\varphi}\left|U_{\perp}(k_x - k_w\cos\varphi, k_y - k_w\sin\varphi)\right|^2$ in Eq. (25) is a shifted version with weight a_{φ} of the FP image that would be observed under traditional perpendicular out-of-plane illumination. Therefore, one can find, from the distribution of points where $\left|U_{\perp}(\vec{k})\right| \neq 0$, the distribution of reciprocal space points $\left(k_x, k_y\right)$ where $I_T(\vec{k}) \neq 0$. In order to achieve this, one can imagine, as shown in Fig. 4, a vector $\overrightarrow{k_w}$ attached to each point $\left(k_x^{'}, k_y^{'}\right)$ such that $\left|U_{\perp}(k_x^{'}, k_x^{'})\right| \neq 0$ (represented by red dots in Fig. 4). When the direction φ of the surface wave illumination changes from 0 to 2π, the vectors $\overrightarrow{k_w}$ rotate simultaneously around their origins. This resulting in each point $\left(k_x^{'}, k_y^{'}\right)$ being substituted by a ring of radius k_w centered in that point. The collection of all these rings form the distribution of reciprocal space points $\left(k_x, k_y\right)$ where $I_T(k_x, k_y) \neq 0$. The total intensity distribution in the FP image, $I_{T,FPI}(k_x,k_y)$, is the part of $I_T(k_x, k_y)$ captured by the microscope high *NA* objective lens; i.e.:

$$I_{T,FPI}(k_x,k_y) \begin{array}{ll} =0, & \left|\vec{k}\right| > k_o NA \\ = I_T(k_x,k_y), & \left|\vec{k}\right| \le k_o NA \end{array}. \tag{26}$$

It should be pointed out here that the observation of full rings in the FP images (see instance in Fig. 4) is conditioned by the existence of surface waves traveling in all directions in the medium/PMMA interface. However, this is not always the case. It is well known that two dimensional plasmonic and photonic crystals may have directional gaps [37–39]. Directional gaps are formed when the propagation in the crystal of surface waves are prohibited in a range of directions. When this happen the weight coefficient in Eq. (25) is equal to zero for all prohibited directions.

4. Origin of subwavelength resolution

In the SWIS-microscope arrangement, each surface wave illumination direction φ produces an independent image of the object under observation, $I_{\varphi,SEI}(x,y)$, at the image plane of the microscope. The intensity distribution of this image is given by the following expression:

$$I_{\varphi,SEI}(x,y) \propto \left|U_{\varphi,IP}(x,y)\right|^2, \tag{27}$$

where $U_{\varphi,IP}(x,y)$ is the optical disturbance at the image plane corresponding to $U_{\varphi,FP}(k_x,k_y)$, which is the part of $U_\varphi(\vec{k})$ captured by the microscope lenses, i.e.:

$$U_{\varphi,FP}(k_x,k_y) \begin{array}{ll} =0, & \left|\vec{k}\right| > k_o NA \\ = U_\varphi(k_x,k_y), & \left|\vec{k}\right| \le k_o NA \end{array}. \tag{28}$$

Therefore, $U_{\varphi,IP}(x,y)$ is given by the inverse FT of $U_{\varphi,FP}(k_x,k_y)$, i.e [24]:

$$U_{\varphi,IP}(x,y) \propto FT^{-1}\left[U_{\varphi,FP}(k_x,k_y)\right] \propto \iint U_{\varphi,FP}(k_x,k_y) e^{i\left(xk_x+yk_y\right)} dk_x dk_y. \tag{29}$$

The final intensity distribution in the SE image obtained with the SWIS-microscope arrangement [12,13,15,18,19], $I_{SEI}(x,y)$, is formed by addition of the images corresponding to all directions, i.e.:

$$I_{SEI}(x,y) = \sum_\varphi I_{\varphi,SEI}(x,y). \tag{30}$$

The sum of the intensities corresponding to different directions at the medium/PMMA interface was previously introduced for plasmonic crystals by showing that plasmon-coupled leakage radiation superlenses can be used to directly probe the Bloch wavefunctions of the photons in a two-dimensional crystal [36]. The correspondence between the SE image and the electric field distribution in the medium/PMMA interface is due to the proportionality between E_{lo} in Eq. (4) and $E_{\dagger o}$ in Eq. (2). The origin of the subwavelength resolution capabilities of SWIS [13,15,19] can be better illustrated for simple periodical structures. As discussed above, when $k_w + G \le k_o NA$, the zero and first order rings are observed in the FP image corresponding to a one dimensional periodic structure (see Fig. 4); therefore, using Eqs. (17) and (19), and Eqs. (28)-(29), results:

$$\begin{aligned} U_{\varphi,IP}(x,y) &\propto FT^{-1}\left[U_{\perp,p}(\vec{k}-\overrightarrow{k_w})\right] \\ &\propto FT^{-1}\left\{\delta\left[\vec{k}-\overrightarrow{k_w}\right] + \delta\left[\vec{k}-\left(\overrightarrow{k_w}+\vec{G}\right)\right] + \delta\left[\vec{k}-\left(\overrightarrow{k_w}-\vec{G}\right)\right]\right\}. \end{aligned} \tag{31}$$

Therefore, it follows from the shift property of FT and Eq. (31) that for any illumination direction φ, the absolute value of the optical disturbance at the image plane $U_{\varphi,IP}(x,y)$ is proportional to the optical disturbance that would be at the object plane under traditional perpendicular out-of-plane illumination, i.e.:

$$\left|U_{\varphi,IP}(x,y)\right| \propto \left[1+\sin\left(\tfrac{2\pi}{p}x\right)\right]. \tag{32}$$

From Eqs. (30) and (32) follows that every SE image obtained using directional surface waves illumination, $I_{\varphi,SEI}(x,y)$, independently of the illumination direction φ, matches the image that would be obtained under traditional perpendicular out-of-plane illumination. Therefore, in correspondence with experimental results [18], from Eq. (30) follows than in the case $k_w + G \le k_o NA$, the total intensity distribution in the SE image closely matches the image that would be obtained under perpendicular out-of-plane illumination.

The more interesting case of $k_w + G > k_o NA$ but $k_w - G \le k_o NA$ is depicted in Fig. 5. A schematic illustration of the transversal structure of a plasmonic SWIS (SWIS without metal) is shown in Fig. 5(a) (Fig. 5(b)). The fabrication details of these samples have been published elsewhere [15,19]. The plasmonic SWIS is a plasmonic crystal with square symmetry and period of p = 300 nm formed by patterning the top PMMA + R6G layer; therefore, the patterned air holes with a diameter of 100 nm were the object under observation in this

#186361 - $15.00 USD Received 5 Mar 2013; revised 28 Apr 2013; accepted 3 May 2013; published 8 May 2013

sample [19]. The SWIS without metal is a photonic crystal with square symmetry and period of p = 220 nm formed by ~35 nm thick chromium (Cr) deposited over a ~150 µm thick coverslip substrate. A 110 nm thick layer of PMMA doped with R6G was then spun on top of the whole structure, and finally, in order to increase the subwavelength resolution, a drop of water was placed on top of the fabricated SWIS; therefore, the Cr pillars were the object under observation in this sample [15]. Cr was used here because it does not exhibit a well-defined plasmonic signature, can be simply patterned after deposition on a glass substrate, and it provides high SE contrast images. Therefore we denote the sample sketched in Fig. 5(b) as an SWIS without metal.

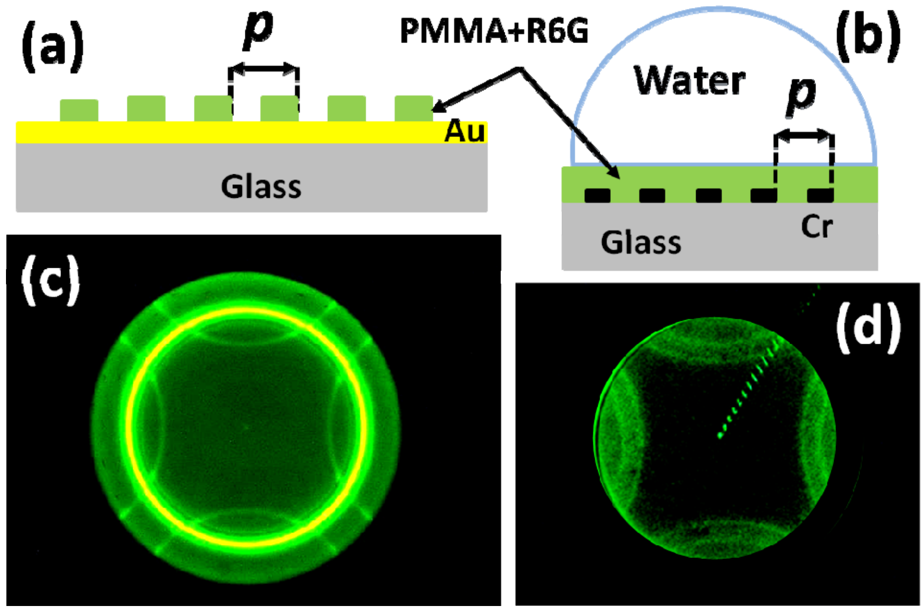

Fig. 5. Schematic illustration of the transversal structure of a (a) plasmonic SWIS, and (b) SWIS without metal. (c) FP image corresponding to the plasmonic SWIS. (d) Intensity distribution inside of the zero order ring resulting from subtracting the FP image corresponding to a homogeneous SWIS without metal, from the FP image corresponding to the SWIS without metal with a periodic patterned structure.

Figure 5(c) shows the FP image obtained with a SWIS-microscope arrangement corresponding to the plasmonic SWIS with the structure sketched in Fig. 5(a). The zero order ring and arc-segments of the first order rings distributed with square symmetry are clearly seen in this image. A similar FP image was obtained using the SWIS without metal with the structure sketched in Fig. 5(b) [15]; however, the first order rings were faint in the image. This indicates that the in-plane scattering of the surface waves was more efficient in the plasmonic SWIS than in the SWIS without metal [34]. Nevertheless, the presence of the faint first order rings is revealed in Fig. 5(d), which shows the intensity distribution inside of the zero order ring, resulting from subtracting the FP image corresponding to the homogeneous SWIS without metal with the structure sketched in Fig. 1(a) (see Fig. 3(b)), from the FP image corresponding to the SWIS without metal with the structure sketched in Fig. 5(b). Similarly to the FP image shown in Fig. 5(c), arc-segments of the thick first order rings distributed with square symmetry are clearly seen in Fig. 5(d).

The graphical compositions shown in Fig. 6 illustrate how the FP images shown in Fig. 5 are formed by the superposition of rings of radius k_w centered at the spots corresponding to the diffraction pattern that would be obtained using traditional perpendicular out-of-plane

#186361 - $15.00 USD Received 5 Mar 2013; revised 28 Apr 2013; accepted 3 May 2013; published 8 May 2013

illumination. Only the arc-segments of these rings captured by the high NA objective lens are observed in the FP image. Neighbors spots are separated in the reciprocal space a distance G = $2\pi/p$. A well-known result of the Abbe's theory of image formation is that the periodic structure of the sample would not appear in the image if the first order spots were not captured by the microscope lenses [2]. This is what happens in the FP images shown in Figs. 5 and 6; therefore, the periodic structures existing in the samples sketched in Fig. 5(a) and 5(b) could not be observed in the SE images that were obtained using traditional perpendicular out-of-plane illumination. This is in correspondence with the minimum observable period of p_{min}~381 nm calculated from (1) with NA = 1.49. However, the periodic structures with period of p = 300 nm and 220 nm sketched in Fig. 5(a) and 5(b), respectively, have been successfully imaged (not shown here) using a SWIS-microscope arrangement [15,19]. Consequently, the subwavelength resolution capabilities of SWIS have already been unambiguously demonstrated.

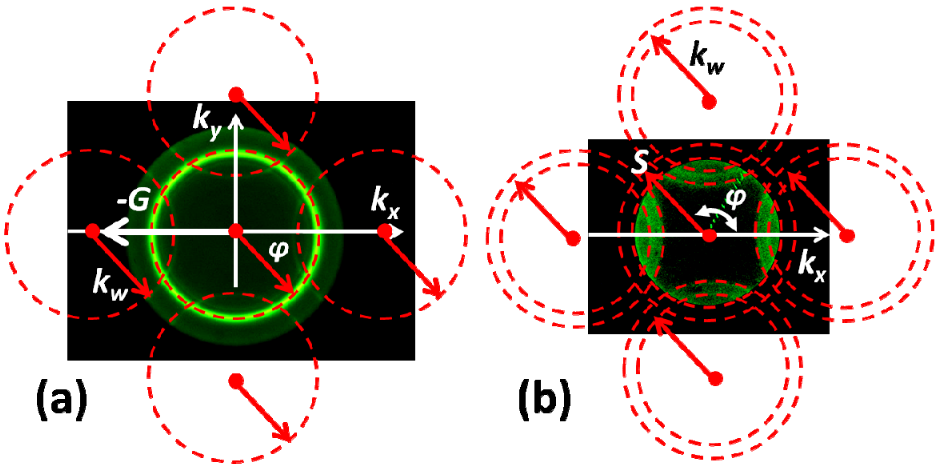

Fig. 6. Graphical composition illustrating how the FP images shown in (a) Fig. 5(c), and 5(b) Fig. 5(d) are formed. The red spots represent the diffraction pattern that would be observed using traditional perpendicular out-of-plane illumination. Similar fractions of the first order rings are observed in both images.

In what follows we will show that the subwavelength resolution capabilities of SWIS can be easily understood using the Fourier optics description of the image formation in a SWIS-microscope arrangement presented above. The diffraction pattern produced by illuminating the samples with surface waves propagating in the direction φ is formed by the five spots pointed by the vectors $\overrightarrow{k_w}$, which are represented by red arrows in Fig. 6. The rings are formed when the vectors $\overrightarrow{k_w}$ rotated around the red spots shown in Fig. 6. Only the diffraction spots captured by the high NA objective lens are observed in the FP image. When φ~3π/4 in the instance illustrated in Fig. 6(b), only the diffraction spot at the reciprocal space point S = $\left(\frac{-\sqrt{2}}{2}k_w, \frac{\sqrt{2}}{2}k_w\right)$ is contained in the region $\left|\vec{k}\right| \le k_o NA$; therefore, using Eq. (29), results:

$$U_{5\pi/4,IP}(x,y) \propto FT^{-1}\left\{\delta\left[\vec{k}-\left(\frac{-\sqrt{2}}{2}k_w, \frac{\sqrt{2}}{2}k_w\right)\right]\right\}. \quad (33)$$

Therefore, from Eqs. (27) and (33) follow that $I_{5\pi/4,SEI}(x,y)$ is constant. This means that the periodic structure in the object under observation cannot be observed in the image formed by using only surface waves propagating in the direction φ = 3π/4. This is exactly what would be seen using traditional perpendicular out-of-plane illumination. Nevertheless, the final

#186361 - $15.00 USD Received 5 Mar 2013; revised 28 Apr 2013; accepted 3 May 2013; published 8 May 2013

intensity distribution in the image is formed by superposition of the images corresponding to all directions. In the instances illustrated in Fig. 6, there are several directions for which first order spots are captured by the microscope objective lens. As a result, the periodic structure of the object under observation is stamped in the final intensity distribution in the image, $I_{SEI}(x,y)$. This is the origin of the subwavelength resolution capabilities of SWIS. Consequently, for a SWIS-microscopy arrangement we can rephrase the traditional enunciate of the Abbe's theory of image formation saying that, *if a fraction of the first order rings can be captured by the high NA objective lens, then the periodic structure of the sample will be visible in the image* [13,15]. This results into the following expressions for the minimum period observable using SWIS [13,15]:

$$p_{SPP,\min} = \frac{\lambda_o}{NA + n_{eff}}, \tag{34}$$

$$p_{TIR,\min} = \frac{\lambda_o}{n_{\sup} + n_{sub}}, \tag{35}$$

where, n_{eff} is the effective refractive index experienced by the excited SPP in plasmonic SWIS; and n_{sub} and n_{sup} are the refractive index of the media below and in top of the medium/PMMA interface in the SWIS without metal. It is worth noting that the minimum period observable is related with the Rayleigh resolution criteria [2] giving the minimum resolvable separation between two points, Δx, by the relation $\Delta x = p_{min}/2$ [1,13,15]. Therefore, from Eq. (1) with NA = 1.49, results a value of $\Delta x \sim \lambda_o/3 \sim 190$ nm; meanwhile, Δx values as small as $\lambda_o/7 \sim 80$ nm have been demonstrated using SWIS [13,15]. Although super-resolution can be achieved for periodic and non-periodic samples [13,19] with any SWIS, the wave excitation choice will depend on several factors such as complexity of sample fabrication, subwavelength resolution limit, and contrast definition of the optical images. For instance, surface waves related to total internal reflection require simpler samples dispensing the need of metal layers when compared to samples investigated by SPP wave excitation. However, it follows from Eq. (34) that deeper subwavelength resolution should be achievable using plasmonic SWIS having a medium/PMMA interface where $n_{eff} >> 1$. Values of n_{eff} much larger than n_{sub} and n_{sup} are possible to obtain in plasmonic SWIS due to non-linear dispersion relation of SPP [16].

5. Conclusions

We have presented, for the first time, a Fourier optics description of the image formation in a SWIS-microscope arrangement. We found an excellent correspondence between the analytical expressions obtained using the Fourier optics approach and the experimental images. We have shown that the same physical principles are responsible for the demonstrated subwavelength resolution capabilities of both plasmonic SWIS and SWIS without metal. In general, SWIS are based in the illumination of the object under observation with surface waves excited by fluorescence, the enhanced transmission of fluorescence via coupling with surface waves, and the occurrence of far-field coherence-related fluorescence diffraction phenomena. Our theoretical approach explains why images with subwavelength resolution can be formed directly in the microscope camera, without involving scanning or numerical post-processing. Finally, we have suggested alternative solutions to obtain deep optical subwavelength resolution with a SWIS-microscope arrangement.

Acknowledgments

This work was partially supported by the NSF CAREER Award (ECCS-0954490).